

# Effect of $ZrO_2$ on the catalytic performance of nano $\gamma-Al_2O_3$ in dehydration of methanol to dimethyl ether at relatively low temperature

Abd El-Aziz A. Said<sup>1</sup> · Mohamed M. M. Abd El-Wahab<sup>1</sup> ·  
Mohamed Abd El-Aal<sup>1</sup>

Received: 12 January 2015 / Accepted: 9 May 2015  
© Springer Science+Business Media Dordrecht 2015

**Abstract** A series of  $ZrO_2/\gamma-Al_2O_3$  catalysts were prepared by incipient wetness impregnation of zirconyl nitrate hydrate aqueous solutions on nano- $\gamma-Al_2O_3$  with  $ZrO_2$  loadings (1–30 % w/w) and calcined at 450 and 550 °C for 3 h in a static air atmosphere. Physicochemical properties of the catalysts were determined using TG, DTA, XRD, FT-IR, Raman spectroscopy, TEM, and  $N_2$  sorption measurements. The surface acidity of the catalysts was investigated by dehydration of isopropanol and adsorption of pyridine, 2,6-dimethyl pyridine and TPD–pyridine. This series of catalysts was used for vapor-phase dehydration of methanol to dimethyl ether in a fixed bed reactor. It was found that all catalysts in this study were active and selective for DME synthesis. According to the experimental results, 1 % ZA catalyst exhibited the highest activity with selectivity of 100 % toward DME.

**Keywords**  $ZrO_2/\gamma-Al_2O_3$  · Methanol · Dehydration · DME

## Introduction

Alumina is an important material in industrial applications and it has a significant importance from the technological point of view. Alumina nanopowders are utilized in many areas of modern industry such as electronics, metallurgy, optoelectronics and fine ceramic composites [1, 2]. Alumina exists in different phases and each phase possesses some unique properties that make it most suitable for special cases. On the other hand, zirconia presents interesting catalytic properties because it is the only metal oxide that demonstrates four chemical properties, on the surface: acidic, basic, oxidizing and reducing properties [3]. The acid and base bifunctional properties of

---

✉ Abd El-Aziz A. Said  
aasaid55@yahoo.com

<sup>1</sup> Chemistry Department, Faculty of Science, Assiut University, Assiut 71516, Egypt

zirconia and its mixed oxides have a number of catalytic properties [4]. However, extensive studies have been carried out on  $\text{ZrO}_2\text{-Al}_2\text{O}_3$  mixed oxides in the heterogeneous catalysis field. They are widely employed as potential catalysts and/or supports for  $\text{NO}_x$  reduction, Fischer–Tropsch synthesis, acetylation of alcohols and amines, catalytic oxidation of hydrocarbons, and isomerization and dehydrogenation reactions, because the mixed system presents higher catalytic behavior than pure  $\text{ZrO}_2$  or  $\text{Al}_2\text{O}_3$  oxides [5]. With the rapid growth of methanol production from coal-derived syngas, the research and the development of new processes to transform methanol into valuable products has attracted extensive attention. Through oxidation and/or dehydration, methanol can be converted to formaldehyde (FA), dimethyl ether (DME), dimethoxymethane (DMM), methyl formate (MF), and so on. Among them, DME is one of the most promising types of diesel fuel since it has a thermal efficiency equivalent to the traditional diesel fuel, lower  $\text{NO}_x$  emission, fewer carbon particulates, and near-zero smoke and laser engine noise [6, 7]. DME can be produced by two methods. The first is considered as the indirect method, in which it is produced by dehydration of methanol over solid acid catalysts [8, 9], and the second one is the direct synthesis of DME from synthesis gas (STD) over a hybrid catalyst comprising a methanol-synthesis catalyst and a solid acid in a single reactor [10, 11]. Commercially, DME is produced by the catalytic dehydration of methanol at around 300 °C at 10 atm pressure over solid catalysts such as  $\gamma\text{-Al}_2\text{O}_3$  or zeolites, combined with different additives [12]. The main problems with the catalysts are coke formation and coating the surface with carbon, which requires their replacement more frequently than is desirable. This necessitates a search for new catalysts with high activity and long periods of exploitation. Undoubtedly, alumina is an excellent candidate for the methanol dehydration process as provided by many reports. However, its unsolved drawbacks are also obvious, such as low hydrothermal activity, many side reactions, competitive adsorption of steam resulting from the strong surface hydrophilic ability, etc. [13]. Recently, numerous researchers have performed a series of effective works to develop an active, selective and stable alumina-based catalyst. Modification with another oxide is considered as one of the most powerful approaches to improve the performance of  $\gamma\text{-Al}_2\text{O}_3$  [13]. However, the effect of  $\text{ZrO}_2$  on the catalytic activity and selectivity of  $\gamma\text{-Al}_2\text{O}_3$  in the dehydration of methanol to DME has to our best knowledge not yet been investigated. Therefore, the aim of the present work is to study the effect of  $\text{ZrO}_2$  contents upon the catalytic performance of nano  $\gamma\text{-Al}_2\text{O}_3$  catalyst for methanol dehydration to DME at relatively low temperature (230 °C) under inert and oxidative atmosphere. In addition, we have investigated the correlation between the activity and the acid properties of the prepared catalysts.

## Experimental

### Catalyst preparation

Aluminum nitrate nonahydrate  $\text{Al}(\text{NO}_3)_3 \cdot 9\text{H}_2\text{O}$  (Oxford assay 98.5 %), zirconyl nitrate hydrate  $\text{ZrO}(\text{NO}_3)_2 \cdot x\text{H}_2\text{O}$  (Aldrich), ammonia solution ( $\text{NH}_4\text{OH}$  23 %), methyl alcohol, isopropyl alcohol, pyridine and 2,6-dimethyl pyridine were obtained

as pure reagents and were used without further purification. Calculated amount of aluminum nitrate nonahydrate with concentration of 0.5 M was dissolved in distilled water at 60 °C with continuous stirring by a magnetic stirrer then drop-wise addition of ammonia solution until the pH equalled 7. After that, the precipitated solution was filtered and washed by distilled water to remove nitrate ions and excess ammonia. The precipitate was dried in an oven at 100 °C for 24 h and calcined at 500 °C in a static air atmosphere for 3 h. The samples of ZrO<sub>2</sub> supported on  $\gamma$ -Al<sub>2</sub>O<sub>3</sub> were prepared by the impregnation method. Calculated amounts of zirconyl nitrate hydrate were dissolved in small amounts of distilled water. The zirconyl nitrate hydrate solutions were admixed carefully with calculated amounts of nano- $\gamma$ -alumina until the formation of homogeneous pastes. The mixtures were dried in an oven at 100 °C for 24 h, when the contents of ZrO<sub>2</sub> were 1–30 wt%. All the supported samples were calcined at 450 and 550 °C for 3 h in a static air atmosphere. This series of  $\gamma$ -Al<sub>2</sub>O<sub>3</sub> samples with 1–30 wt% ZrO<sub>2</sub> loading, were named (1–30) % ZA.

## Catalyst characterization

### *Thermal analysis*

Thermogravimetry (TG) and differential thermal analysis (DTA) were performed on heating (at 10 °C min<sup>-1</sup>) test samples to 800 °C in a dynamic atmosphere of air (30 mL min<sup>-1</sup>) using a computerized Shimadzu Thermal Analyzer TA60 Apparatus (Japan).

### *X-ray diffraction (XRD)*

XRD analysis of the test samples was performed with a Philips (Netherlands) diffractometer (Model PW 2103,  $\lambda = 1.5418 \text{ \AA}$ , 35 kV and 20 mA) with a source of CuK $\alpha$  radiation (Ni filtered). An online data acquisition and handling system facilitated the automatic JCPDS library search and match for phase identification purposes. Patterns were recorded from 4° to 80° (2 $\theta$ ). Particle size was estimated using the Scherrer equation [14]

$$D = \frac{K\lambda}{\beta \cos\theta}$$

where  $D$  is the mean crystallite diameter (nm),  $\lambda$  is the X-ray wavelength,  $K$  is the Scherrer constant (0.89), and  $\beta$  is the observed angular width at half maximum intensity of the peak.

### *Fourier transform infrared (FT-IR) spectroscopy*

FT-IR spectra of the prepared catalysts calcined at 450 and 550 °C for 3 h were recorded using a Nicolet spectrophotometer (model 6700), equipped with a data station in the range of 4000–400 cm<sup>-1</sup> with a KBr disc technique.

### *Raman spectroscopy*

Raman spectra of the prepared catalysts calcined at 450 °C were obtained using Raman spectroscopy model SENTERRA Inverted Configuration (Germany) under ambient conditions, e.g. 25 °C. A 785 nm laser was used as the exciting source on the sample surface with a power of 50 mW.

### *Transmission electron microscopy (TEM)*

The size and morphology of the investigated catalysts were characterized by transmission electron microscope (TEM) JEOL Model JSM-5400 LV (Joel, Tokyo, Japan). The catalyst powder dispersed in ethanol using ultrasonic radiation for 20 min and a drop of that suspension was placed onto the carbon-coated grids. The degree of magnification of TEM images was the same for all the different investigated catalysts.

### *Nitrogen gas sorption*

Nitrogen gas adsorption–desorption isotherms were measured at  $-196$  °C using a Nova 3200 instrument (Quantachrom Instrument, USA). Test samples were thoroughly outgassed for 3 h at 250 °C to a residual pressure of  $10^{-5}$  Torr, and the weight of the degassed sample was that used in calculations. The specific surface area,  $S_{\text{BET}}$  was calculated by applying the Brunauer–Emmett–Teller (BET) equation. The porosity of the catalysts was determined from the desorption curves using Nova enhanced data reduction software (v.2.13).

### *Acidity determination*

The acidity of the catalysts under investigation was determined by studying the dehydration of isopropyl alcohol (IPA) and the adsorption of pyridine (PY), 2,6-dimethyl pyridine (DMPY). The dehydration of IPA was carried out in a conventional fixed-bed flow Pyrex glass tube reactor, at atmospheric pressure using nitrogen as a carrier gas. The reaction conditions were: 500 mg catalyst weight, 2 % IPA in the gas feed, 50 mL min<sup>-1</sup> total flow rate and 180 °C reaction temperature. The measurement of propene yield (%) was made after 1 h to achieve steady-state reaction conditions of the IPA. The chemisorptions of PY and DMPY were carried out by injection of different volumes at steady-state conditions. The exit feed was analyzed by direct sampling of the gaseous products into a Unicam ProGC gas chromatograph using a flame ionization detector (FID) with a 10 % PEG 400 glass column (2 m). The acidity populations over the surface of catalysts, under investigation, were also measured by thermogravimetric technique (TG) using the adsorption of pyridine as probe molecule. The following procedure was used: 500 mg of calcined sample was preheated at 250 °C for 1 h in air before being saturated with pyridine for 7 days after evacuation, then 10–15 mg of pyridine-saturated sample was subjected to TG and DTA analysis. The analysis was recorded by heating from room temperature to 400 °C at 10 °C min<sup>-1</sup> and 30 mL min<sup>-1</sup> flow of N<sub>2</sub>. The mass loss due to desorption of pyridine from the acidic sites was determined as a function of total surface acidity [15].

### Catalytic activity measurements

The catalytic activity of the catalysts for the vapor-phase dehydration of methyl alcohol was carried out at 230 °C in a conventional fixed bed flow type reactor at atmospheric pressure using air or nitrogen as a carrier gas. The measurement procedure was similar to that reported previously [16]. Each catalytic run was conducted using 500 mg of the powdered catalyst and a total flow rate was fixed at 50 mL  $\text{min}^{-1}$  and 4 % methanol in the gas feed. The gases after reaction were chromatographically analyzed by FID with a Unicam ProGC using a 2-m DNP glass column for analysis of the reaction products of methyl alcohol on the tested catalysts. Measurements of the conversion and yield (%) were recorded after 1 h from the initial introduction of the reactant into the reactor to ensure the attainment of the reaction equilibrium, (steady-state conditions).

## Results and discussion

### Thermal analysis

TG and DTA curves for the prepared  $\gamma\text{-Al}_2\text{O}_3$  calcined at 500 °C and 10, 20 and 30 % ZA catalyst original precursors are represented in Fig. 1. The TG and DTA curves for all samples exhibit two weight loss steps. The first one is in the range of

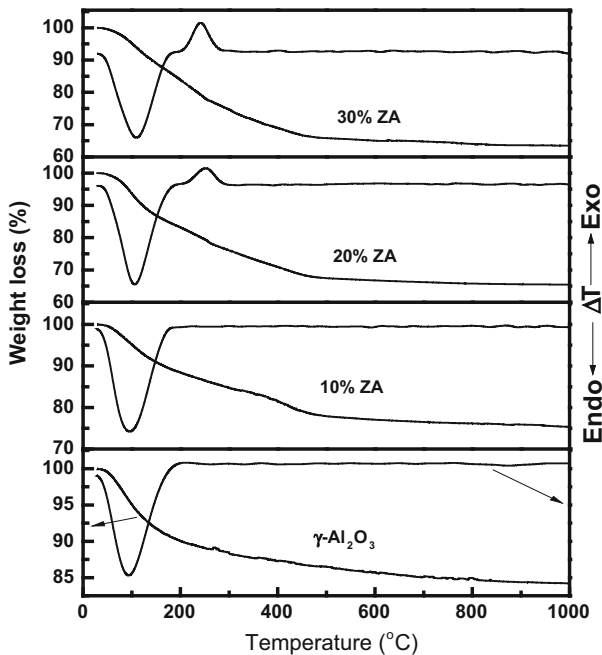


**Fig. 1** TG and DTA curves for the prepared  $\gamma\text{-Al}_2\text{O}_3$  calcined at 500 °C, for 10, 20 and 30 % ZA original precursors

30–200 °C with a weight loss of 10, 11.6, 16.1 and 16.8 %, respectively. The samples also exhibit endothermic peaks appear on the DTA profiles minimized at 89, 99, 103 and 111 °C for  $\gamma$ - $\text{Al}_2\text{O}_3$ , for 10, 20 and 30 % ZA catalysts, respectively. These peaks attributed to the loss of physically adsorbed and crystalline water molecules. The second step occurs in the range of 200–800 °C with weight loss of 5.1, 6.9, 12.3 and 17.9 for  $\gamma$ - $\text{Al}_2\text{O}_3$ , for 10, 20 and 30 % ZA catalysts, respectively. This step was not accompanied by any peak in the DTA curves of  $\gamma$ - $\text{Al}_2\text{O}_3$  and 10 % ZA catalyst, while 20 and 30 % ZA catalysts exhibited exothermic peaks maximized at 251 and 241 °C for 20 and 30 % ZA, respectively. These peaks may be attributed to a certain change in the structure of  $\text{ZrO}_2$  (dehydroxylation process) [17].

### X-ray diffraction (XRD)

XRD patterns determined for the various alumina supported  $\text{ZrO}_2$  catalysts with 10, 20 and 30 wt% loadings and calcined at 450 °C are illustrated in Fig. 2. Matching the XRD patterns of pure  $\gamma$ - $\text{Al}_2\text{O}_3$  calcined at 500 °C with that identified in the (JCPDS NO. 290063) results show that the predominant diffraction peaks correspond to  $\gamma$ - $\text{Al}_2\text{O}_3$  are at  $2\theta = 37.4^\circ$ ,  $46^\circ$  and  $66.5^\circ$ . The XRD patterns of

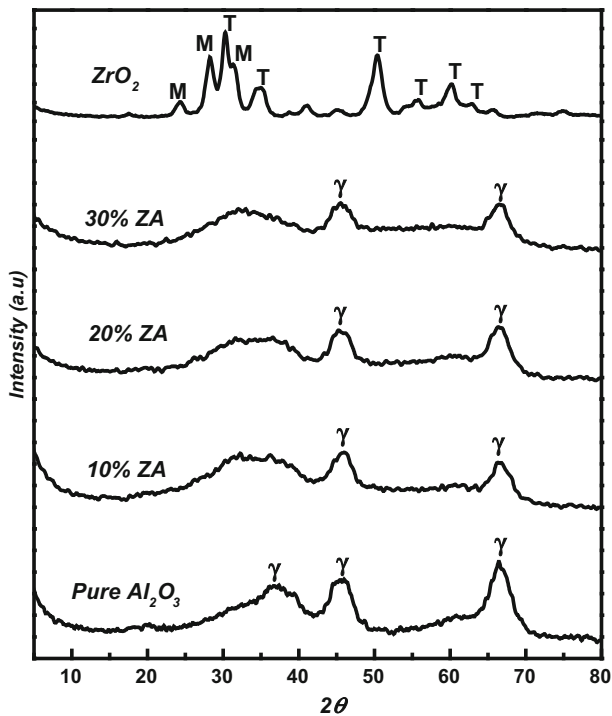


**Fig. 2** X-ray diffraction of pure  $\gamma$ - $\text{Al}_2\text{O}_3$  calcined at 500 °C, pure  $\text{ZrO}_2$  and 10, 20 and 30 % ZA calcined at 450 °C

pure zirconia calcined at 450° exhibit both tetragonal ( $2\theta = 30.3^\circ, 35.3^\circ, 50.7^\circ, 59.9^\circ, 60.6^\circ$  and  $63.5^\circ$  [18]) and monoclinic ( $2\theta = 24.7^\circ, 28.4^\circ, 31.6^\circ$  [19]) phases. However, the XRD patterns of 10, 20 and 30 % ZA calcined at 450° showed reflections typical of the  $\gamma$ -Al<sub>2</sub>O<sub>3</sub> phase. The intensity of the diffraction peaks of the  $\gamma$ -Al<sub>2</sub>O<sub>3</sub> decrease with increasing zirconia contents. The samples also showed a broadened peak at  $2\theta \approx 30^\circ$ , and the intensity of the peak increased with increasing zirconia contents. The broadened peak was attributed to the tetragonal phase zirconia [20], but it was also considered as an appearance of amorphous zirconia [21]. The diffraction peaks at  $2\theta$  values of  $50.7^\circ$  and  $66.46^\circ$  were selected for calculating the crystalline size for pure ZrO<sub>2</sub> and pure  $\gamma$ -Al<sub>2</sub>O<sub>3</sub> phases, respectively. The crystalline sizes for pure ZrO<sub>2</sub> calcined at 450 °C and pure  $\gamma$ -Al<sub>2</sub>O<sub>3</sub> calcined at 500 are cited in Table 1. The results obtained reveal that the addition of ZrO<sub>2</sub> to  $\gamma$ -Al<sub>2</sub>O<sub>3</sub> leads to increase in the crystallite size of  $\gamma$ -Al<sub>2</sub>O<sub>3</sub> phase.

### Fourier transform infrared (FTIR) spectroscopy

The FTIR spectra obtained for pure nano  $\gamma$ -Al<sub>2</sub>O<sub>3</sub> calcined at 500 °C, pure ZrO<sub>2</sub> and the different loadings of ZrO<sub>2</sub> on nano  $\gamma$ -Al<sub>2</sub>O<sub>3</sub> calcined at 450 °C are shown in Fig. 3. The FTIR spectrum of nano- $\gamma$ -Al<sub>2</sub>O<sub>3</sub> calcined at 500 °C shows a strong and broad band at  $3500\text{ cm}^{-1}$  which is believed to be associated with the stretching vibrations of hydrogen-bonded surface water molecules and hydroxyl groups. Additionally, the bands at  $1633, 1400$  and  $1384\text{ cm}^{-1}$  correspond to the existence of a large number of residual hydroxyl groups, which implies that the O–H vibration mode of the traces adsorbed water. The band located at  $610\text{--}883\text{ cm}^{-1}$  can be ascribed to the Al–O vibration of Al<sub>2</sub>O<sub>3</sub>. These results are in good agreement with

**Table 1** The specific surface areas, pore characteristics and crystalline sizes of the ZrO<sub>2</sub>–Al<sub>2</sub>O<sub>3</sub> samples calcined at 450 and 550 °C

Calcination temp. % ZrO <sub>2</sub>	450 °C				550 °C		
	SBET m <sup>2</sup> g <sup>-1</sup>	Total pore volume (cc g <sup>-1</sup> )	Average pore diameter (nm)	DXRD (nm) <sup>a</sup>	SBET m <sup>2</sup> g <sup>-1</sup>	Total pore volume (cc g <sup>-1</sup> )	Average pore diameter (nm)
Pure Al <sub>2</sub> O <sub>3</sub>	222	0.28485	5.1	8.0	202	0.29376	5.8
1	244	0.31863	5.2	–	204	0.29747	5.8
3	241	0.30794	5.1	–	203	0.29271	5.7
5	229	0.29912	5.2	–	199	0.29763	6.0
7	221	0.28888	5.2	–	200	0.28726	5.7
10	235	0.29697	5.0	9.00	203	0.29140	5.7
20	230	0.28697	5.0	10.0	180	0.24780	5.5
30	198	0.24340	4.9	10.5	168	0.21734	5.1
Pure ZrO <sub>2</sub>	86.2	0.13486	6.2	11.0	49.2	0.14552	11.8

<sup>a</sup> Crystalline size: determined by XRD results

the results obtained by Zhang et al. [22]. The FTIR spectrum of pure  $\text{ZrO}_2$  shows that bands assigned at  $490\text{--}745\text{ cm}^{-1}$  correspond to the O–Zr bond [23]. A strong and broad band assigned at  $3600\text{--}3000\text{ cm}^{-1}$  may correspond to physisorbed water, whereas the band at  $1633\text{ cm}^{-1}$  was assigned to the bending mode ( $\nu_{\text{HOH}}$ ) of coordinated water [24]. In addition, the band at  $1362\text{ cm}^{-1}$  was assigned to the bending vibration of Zr–OH groups [25]. The FTIR spectra of the different loadings of  $\text{ZrO}_2$  on nano- $\gamma\text{-Al}_2\text{O}_3$  calcined at  $450\text{ }^\circ\text{C}$  indicate that the positions of all peaks showed no apparent change. However, the intensities of the peaks were decreased. It should be noted that the peaks of Zr–O do not exist. This is possibly due to the stronger intensity of Al–O vibration than that of Zr–O vibration, thereby the peak of Zr–O vibration is masked [26], which is due to the dispersion of  $\text{Zr}^{4+}$  ions within the alumina lattice, substituting  $\text{Al}^{3+}$  ions. Finally, there is a small band present at  $2170\text{ cm}^{-1}$ , which has been assigned to the Zr–O–Al bond vibration [5, 27]. This band can also be observed in pure  $\gamma\text{-Al}_2\text{O}_3$  sample. Therefore, it should correspond to the M–O–M' band vibration, where M and M' may be the same element or

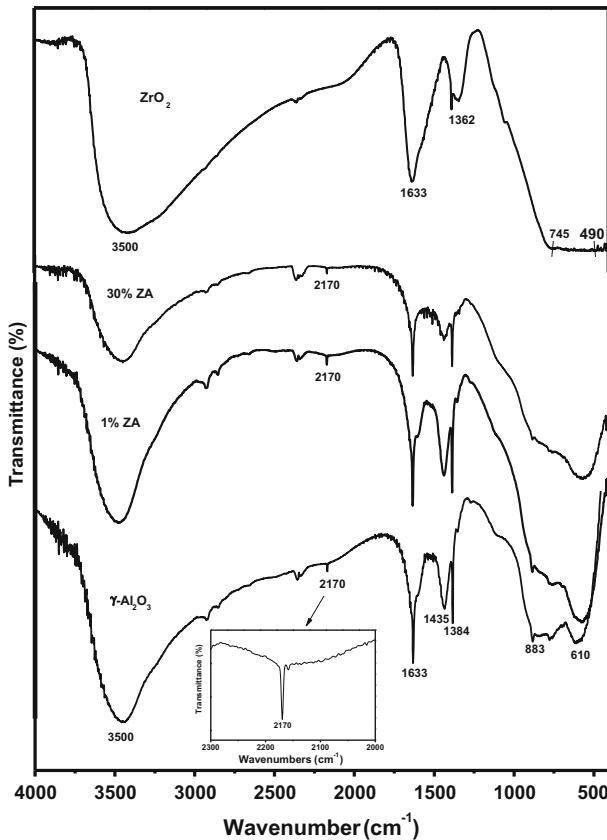


**Fig. 3** FTIR spectra of pure  $\gamma\text{-Al}_2\text{O}_3$  calcined at  $500\text{ }^\circ\text{C}$ , pure  $\text{ZrO}_2$ , for 1 and 30 % ZA catalysts calcined at  $450\text{ }^\circ\text{C}$

different elements, such as Al–O–Al or Zr–O–Zr. In addition, the FTIR spectra of the samples calcined at 550 °C (not shown) show the same bands as in the samples calcined at 450 °C but with a slight decrease in their intensities.

### Raman spectroscopy

The Raman spectra of pure  $\gamma$ -Al<sub>2</sub>O<sub>3</sub> calcined at 500 °C, for 1 and 30 % ZA catalysts calcined at 450 °C, are presented in Fig. 4. The laser Raman spectra of  $\gamma$ -Al<sub>2</sub>O<sub>3</sub> calcined at 500 °C does not exhibit any Raman peaks [28], but the addition of 1 % ZrO<sub>2</sub> produced a peak at about 970 cm<sup>-1</sup>. This peak may be attributed to vibrational modes involving Zr–O–Al linkages. The intensity of this peak increased on increasing the percentages loading up to 30 % ZA. The results are in a good agreement with those obtained by Gao et al. [29].

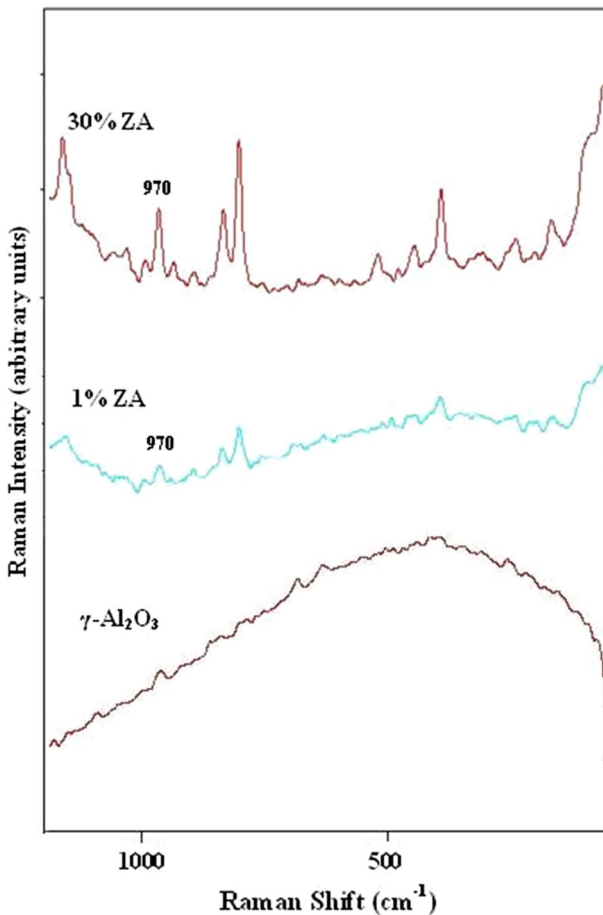


**Fig. 4** Raman spectra of pure  $\gamma$ -Al<sub>2</sub>O<sub>3</sub> calcined at 500 °C, for 1 and 30 % ZA catalysts calcined at 450 °C

## Transmission electron microscopy (TEM)

To obtain more information about the morphological features of synthesized  $\gamma$ - $\text{Al}_2\text{O}_3$ , 1 and 30 % ZA catalysts, TEM studies were undertaken as shown in Fig. 5. A TEM image of  $\gamma$ - $\text{Al}_2\text{O}_3$  calcined at 500 °C shows the presence of small aggregates with average particle size of about 8.4–14 nm. The average particle size calculated from the TEM micrographs is consistent with the average crystalline size obtained from XRD measurement as indicated in Table 1. On the other hand, a TEM image of 1 and 30 % ZA catalysts calcined at 450 °C shows more fine aggregates.

## Sorption measurements

Adsorption–desorption isotherms of pure  $\text{Al}_2\text{O}_3$  calcined at 500 °C, pure  $\text{ZrO}_2$  and  $\text{ZrO}_2$  supported on  $\gamma$ - $\text{Al}_2\text{O}_3$  catalysts calcined at 450 °C are represented in Fig. 6a. All isotherms of pure and mixed calcined samples resulted in type IV of Brunauer's classification [30]. The type IV isotherm is characteristic of mesoporous materials, in which capillary condensation and the multilayer adsorption (for higher pressure)

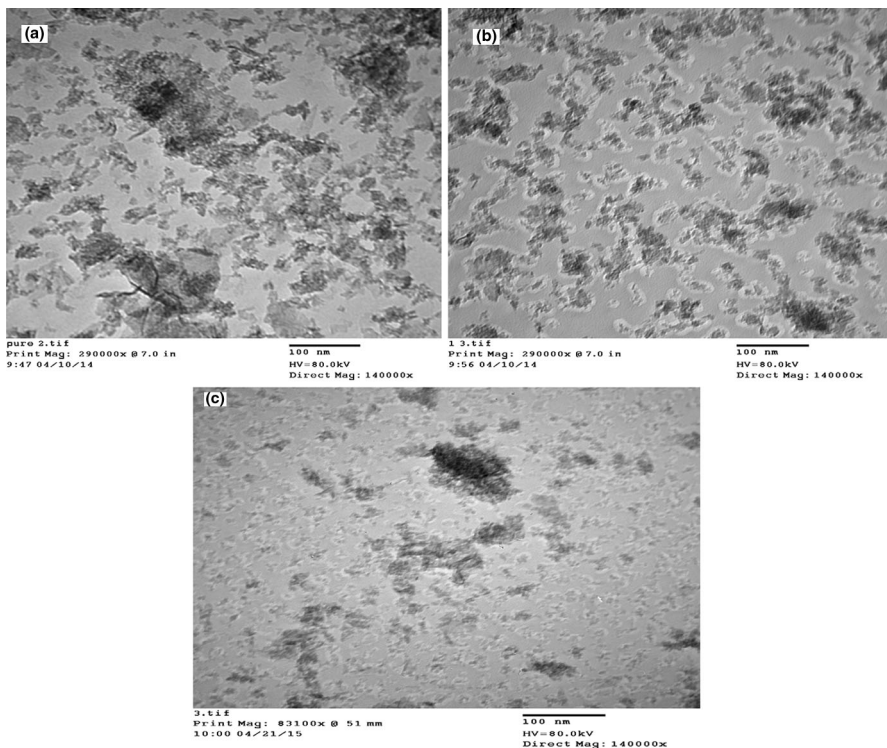


**Fig. 5** TEM images of **a**  $\gamma$ - $\text{Al}_2\text{O}_3$  calcined at 500 °C, **b** 1 % ZA and 30 % ZA catalysts calcined at 450 °C

take place. The hysteresis loop belongs to type H2 of the de Bore classification [31]. The surface areas ( $S_{\text{BET}}$ ), the pore volumes and the average pore diameters of the catalysts are summarized in Table 1. It is clear from Table 1 that pure  $\gamma\text{-Al}_2\text{O}_3$  calcined at 500 and 550 °C has  $S_{\text{BET}}$  values of 222 and 202  $\text{m}^2 \text{g}^{-1}$ , respectively, while pure zirconia calcined at 450 and 550 °C has  $S_{\text{BET}}$  values of 86.2 and 49.2  $\text{m}^2 \text{g}^{-1}$ , respectively. The results also show that, on addition of 1 %  $\text{ZrO}_2$  into  $\gamma\text{-Al}_2\text{O}_3$ , the surface area increased to 244 and 204  $\text{m}^2 \text{g}^{-1}$  for the samples calcined

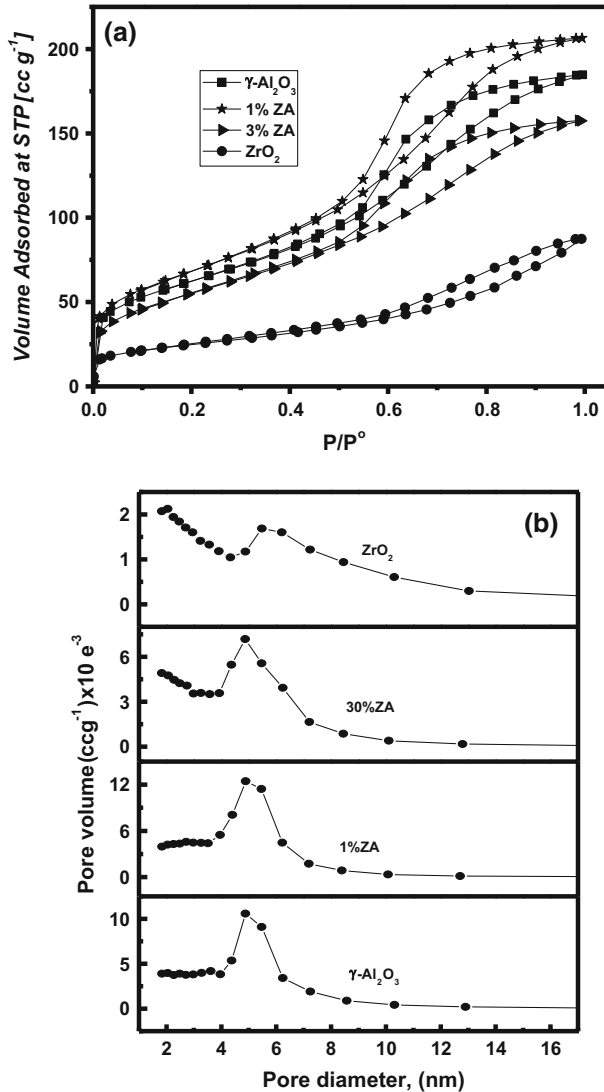


**Fig. 6** a Nitrogen adsorption–desorption isotherms and b the pore size distribution of  $\gamma\text{-Al}_2\text{O}_3$  calcined at 500 °C, pure  $\text{ZrO}_2$ , for 1 and 30 % ZA catalysts calcined at 450 °C

at 450 and 550 °C, respectively, which might be due to the dispersion of the zirconia phase into the alumina phase, leading to structural stabilization [32]. Further addition of  $\text{ZrO}_2$  leads to a continuous decrease in the  $S_{\text{BET}}$  values. However, the 10 % ZA sample provided a higher  $S_{\text{BET}}$  value than the 5 and 7 % ZA. Possibly, this was due to the different particle size of  $\text{ZrO}_2$  in the pores of the alumina [17]. On the other hand, it is observed that the  $S_{\text{BET}}$  of the prepared catalysts decreased with increasing the calcination temperature from 450 to 550 °C. This behavior may be attributed to the sintering process [33]. The pore size distribution curves of  $\gamma\text{-Al}_2\text{O}_3$ ,  $\text{ZrO}_2$  for 1 and 30 % ZA are shown in Fig. 6b. It shows that the pores of  $\gamma\text{-Al}_2\text{O}_3$  have a narrow pore distribution in the range of 4–7.5 nm, while the pores of  $\text{ZrO}_2$  exhibit a minor contribution for mesopores with an average pore diameter of 6 nm and a major contribution for narrow pores of diameter 1.9 nm. In addition, the pore size distribution of 1 % ZA shows a monomodal with wider pore distribution slightly more than pure  $\gamma\text{-Al}_2\text{O}_3$ . Further increasing the contents of  $\text{ZrO}_2$ , the samples exhibit bimodal size distribution as observed in 30 % ZA.

## Determination of the surface acidic sites

### *Dehydration of isopropyl alcohol (IPA)*

The catalytic dehydration of IPA over pure  $\gamma\text{-Al}_2\text{O}_3$  calcined at 500 and 550 °C and the different loadings of  $\text{ZrO}_2$  on  $\gamma\text{-Al}_2\text{O}_3$  catalysts calcined at 450 and 550 °C are shown in Fig. 7. IPA dehydration has been used by several authors [34], as a test reaction to determine the acidity of different catalysts and it proceeds quickly on weak acid sites [35]. Under our working conditions, it was found that IPA reacts on  $\gamma\text{-Al}_2\text{O}_3$  and selectively on the different loadings catalysts to propene. The results indicate that pure  $\gamma\text{-Al}_2\text{O}_3$  calcined at 500 °C exhibits conversion and yield of propene  $\approx 70$  %. Moreover, in the samples calcined at 450 °C, the addition of

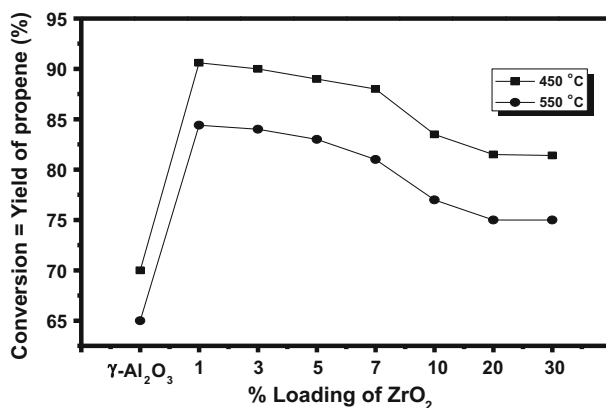


**Fig. 7** Activity variation of IPA with different loadings of  $\text{ZrO}_2$  on  $\gamma\text{-Al}_2\text{O}_3$  calcined at 450 and 550 °C

1 wt% ZrO<sub>2</sub> leads an observable increase in the yield of propene by  $\approx 90.6$  % (maximum yield). Above this ratio, further addition steadily decreases the yield of propene reaches  $\approx 81.4$  % over 30 % ZA catalyst. The decrease in the activity of the catalysts in high zirconia contents may be related to the fact that pure zirconia is an inactive catalyst toward IPA dehydration. The catalysts calcined at 550 °C exhibit the same behavior as the catalysts calcined at 450 °C but exhibit lower activity towards propene formation, due to the decrease in the surface area (see Table 1). The above results show that the catalyst containing 1 wt%. ZrO<sub>2</sub> has sufficient acid sites to proceed the dehydration pathway for IPA better than that of the  $\gamma$ -Al<sub>2</sub>O<sub>3</sub> catalyst. The difference between the performances of 1 % ZA and  $\gamma$ -Al<sub>2</sub>O<sub>3</sub> catalysts is explained on the basis of ZrO<sub>2</sub> interacting with  $\gamma$ -Al<sub>2</sub>O<sub>3</sub> via creation of more acidic sites, which is responsible for the dehydration reaction.

*Poisoning of acid sites with pyridine and 2,6-dimethyl pyridine over  $\gamma$ -Al<sub>2</sub>O<sub>3</sub> and 1 % ZA catalysts during the reaction of IPA*

It is known that the chemisorptions of pyridine (PY) and 2,6-dimethyl pyridine (DMPY) can be used as basic probe molecules to determine the acidity of the catalyst [36]. It has been reported that PY is selectively adsorbed on both Brønsted (B) and Lewis (L) acid sites [37]. On the other hand, DMPY is selectively adsorbed on Brønsted acid sites [38] but not Lewis sites because of the steric hinderance of two methyl groups. So the difference between PY and DMPY adsorption is a measure of the Lewis acid sites. The poisoning of the active surface sites of  $\gamma$ -Al<sub>2</sub>O<sub>3</sub> and 1 % ZA catalysts in IPA conversion was performed through saturation of the acid sites with PY or DMPY according to the following procedure. After measuring the conversion activity of  $\gamma$ -Al<sub>2</sub>O<sub>3</sub> and 1 % ZA catalysts at 180 °C, the catalysts were injected with different volumes of PY or DMPY in the stream of reactants using N<sub>2</sub> as a carrier gas. We selected 1 % ZA catalyst for the poisoning test because it is the most active and selective catalyst in both IPA and methanol dehydration reaction. The results obtained are shown in Fig. 8a. It shows the influence of PY and DMPY additions on the reaction products of IPA over  $\gamma$ -Al<sub>2</sub>O<sub>3</sub> calcined at 500 °C. The results indicate that PY and DMPY suppressed IPA dehydration activity. Thus, the chemisorbed PY and DMPY decreased the yield of the propene by  $\approx 45$  and 7 %, respectively. It is clear from the above results that the difference between the amounts adsorbed from PY and DMPY equal 38 %. This value corresponds to the (L) acid sites present on the surface of the  $\gamma$ -Al<sub>2</sub>O<sub>3</sub> catalyst. Thus, the  $\gamma$ -Al<sub>2</sub>O<sub>3</sub> catalyst is an acidic catalyst with major (L) and minor (B) acid sites. Fig 8a also shows the effect of PY and DMPY additions on the reaction products of IPA over the 1 % ZA catalyst calcined at 450 °C. The results revealed that PY and DMPY retard IPA dehydration activity. Thus, the chemisorbed PY and DMPY decrease the yield of the propene by 56 and 12 %, respectively. The difference between the amounts adsorbed from PY and DMPY is  $\approx 44$  %. This value corresponds to the presence of the (L) acid sites. Thus, the 1 % ZA catalyst is an acidic catalyst with major (L) and minor (B) acid sites. Inspection of the above results illustrate that the number of acidic sites and its distribution present on the surface of 1 % ZA catalyst is greater than that on the surface of  $\gamma$ -Al<sub>2</sub>O<sub>3</sub> catalyst.

### Thermal analysis of $\gamma$ -alumina and 1 % ZA catalysts presaturated with pyridine

To identify the strength of acid sites available on the surface of the catalysts under investigation, thermal analysis of presaturated samples with PY was carried out. Figure 9a depicts the TG and DTA curves of the pyridine removed from  $\gamma$ -Al<sub>2</sub>O<sub>3</sub> catalyst calcined at 500 °C. The TG curve exhibits a total weight loss of about 19.2 % through two steps. The first step lies in the temperature range of 25–120 °C with a weight loss of about 12.3 %. This step is associated with a strong endothermic peak on the DTA profile minimized at 71 °C. This peak may be attributed to the removal of physically adsorbed water and desorption of PY molecules from weak acid sites. The second step lies in the temperature above 120 °C with a weight loss of about 6.9 %. This step is not accompanied by any peak in the DTA curve. This behavior may indicate that the removal of PY from intermediate acid sites occurs without gain or release energy. On the other hand, Fig. 9b also shows the TG and DTA curves of the desorption of pyridine from 1 % ZA catalyst calcined at 450 °C. The TG curve exhibits a total weight loss of about 22.7 % within two steps. The first step occurs in the temperature range of 25–120 °C with a weight loss of about 16.4 %. This step is accompanied by a strong endothermic peak on the DTA curve minimized at 73 °C. This step may also be attributed to the removal of physically adsorbed water and desorption of PY from weak acid sites. The second step lies in the temperature above 120 °C with a weight loss of about 6.3 %. This step is not associated with any peak in the DTA profile. The above results demonstrate that the  $\gamma$ -Al<sub>2</sub>O<sub>3</sub> and 1 % ZA catalysts contain weak and intermediate acid sites, and the percent of strong acid sites is very small. The

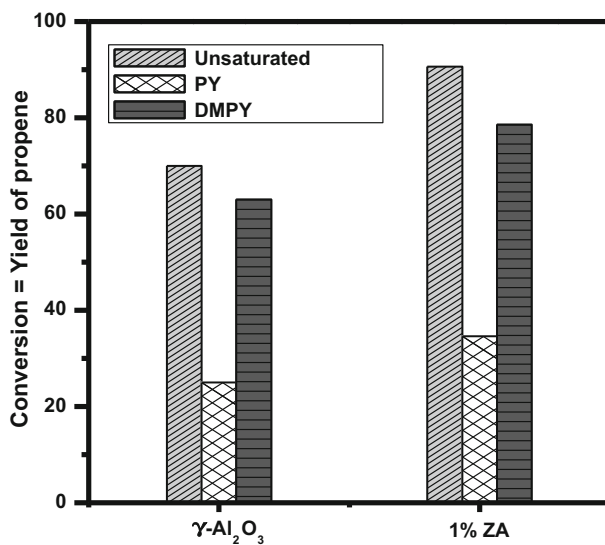


**Fig. 8** Activity variation of IPA with the volume of PY and DMPY over pure  $\gamma$ -Al<sub>2</sub>O<sub>3</sub> calcined at 500 °C and 1 % ZA catalyst calcined at 450 °C (500 mg catalyst, 2 % IPA, 50 mL min<sup>-1</sup> total flow rate, 180 °C reaction temperature)

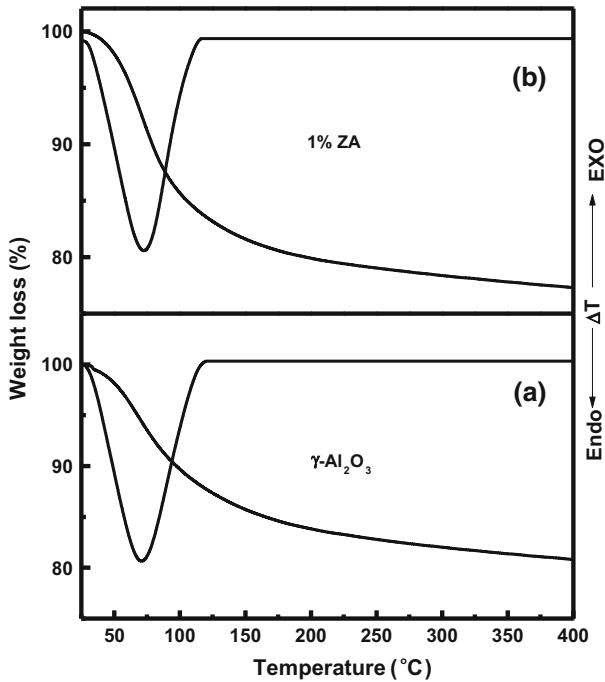


**Fig. 9** TG and DTA curves of PY desorption from (a)  $\gamma$ -Al<sub>2</sub>O<sub>3</sub> and (b) 1 % ZA catalysts

acid site density of  $\gamma$ -Al<sub>2</sub>O<sub>3</sub> and 1 % ZA catalysts were calculated and found to be  $6.56 \times 10^{18}$  and  $7.08 \times 10^{18}$  sites m<sup>-2</sup>, respectively. This indicates that the acid site density (number of acid sites) of 1 % ZA catalyst is more than that of  $\gamma$ -Al<sub>2</sub>O<sub>3</sub>. The above results are in good agreement with the results obtained and presented in Fig. 8.

### Catalytic dehydration of methanol to DME

The catalytic dehydration of methanol over  $\gamma$ -Al<sub>2</sub>O<sub>3</sub> (calcined at 500 and 550 °C) and the different loadings of ZrO<sub>2</sub> on  $\gamma$ -Al<sub>2</sub>O<sub>3</sub> catalysts calcined at 450 and 550 °C using air or nitrogen as a carrier gas are presented in Fig. 10. However, we confirmed previously that using air or nitrogen as a carrier gas gives the same yield of DME with selectivity to DME 100 % over sulfated zirconia samples [16]. The results revealed that pure  $\gamma$ -Al<sub>2</sub>O<sub>3</sub> calcined at 500 and 550 °C exhibits 81 and 79 % conversion of methanol, respectively, with selectivity of 100 % toward DME. On the addition of 1 wt% ZrO<sub>2</sub>, a noticeable increase in conversion and yield of DME reaches 87 and 85 % in the catalyst calcined at 450 and 550 °C, respectively. In the catalysts calcined at 450 °C, with a further increase of the addition of ZrO<sub>2</sub>, a continuous decrease in the conversion and the yield of DME reaches 84.7 % over 30 % ZA catalyst. While, in the catalysts calcined at 550 °C, a further increase in the contents of ZrO<sub>2</sub> decreases the conversion and the yield of DME to  $\approx$  84 % over

5 % ZA catalyst, then a steady state in the conversion and the yield of DME was observed with increasing the addition up to 30 wt%  $\text{ZrO}_2$ . The formation of DME as the only product indicates that the active sites are mainly Lewis acid pair sites,  $\text{Al}^{3+}\text{-O}^{2-}$  [39]. The methanol interacts with a Lewis acid site,  $\text{Al}^{3+}$ , through its oxygen atom, resulting in the dissociative adsorption forming an  $\text{Al-O-CH}_3$  intermediate and a hydrogen atom adsorbed on a surface oxygen ion. DME then forms as a result of condensation of two neighboring surface methoxy groups [40]. Furthermore, the degree of conversion of methanol increases as the surface acidity increases [41]. Therefore, our results indicate an enhancement in the (L) acidity of 1 % ZA catalyst as compared with the pure  $\gamma\text{-Al}_2\text{O}_3$ . The enhanced acidity of the surface could be referred to the possible formation of  $\text{Zr-O-Al}$  bonds. Such heterolinkage has been suggested in several studies to enhance the acidity in various metal oxide systems [42]. The lower activity of the catalysts with high  $\text{ZrO}_2$  contents may be due to the decrease in the acidity of these catalysts as observed in the acidity test (see Fig. 7). So, the highest catalytic activity of 1 % ZA catalyst may be attributed to the increased number of acid sites, as concluded from Fig. 8, and a high surface area.

Consequently, it is important to study the effects of some parameters on the activity of the most active sample (1 % ZA catalyst) in dehydration of methanol to optimize the best conditions for DME production.

#### *Effect of catalytic reaction temperature*

The effect of reaction temperature on the catalytic dehydration of methanol over 1 % ZA catalyst calcined at 450 °C was carried out using air or nitrogen as a carrier gas in the temperature range of 100–275 °C. The percentages of conversion, yield and selectivity are shown in Fig. 11, which shows that the reaction starts at 125 °C

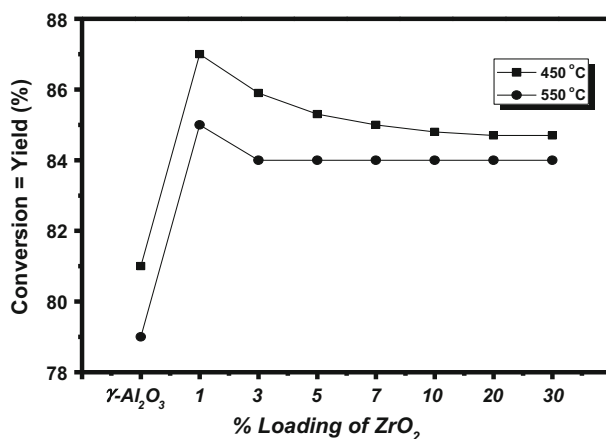


**Fig. 10** Variation of methanol conversion and DME yield over  $\gamma\text{-Al}_2\text{O}_3$  calcined at 500 and 550 °C and the different loadings of  $\text{ZrO}_2$  on  $\gamma\text{-Al}_2\text{O}_3$  catalysts calcined at 450 and 550 °C using air or nitrogen as a carrier gas at 230 °C reaction temperature

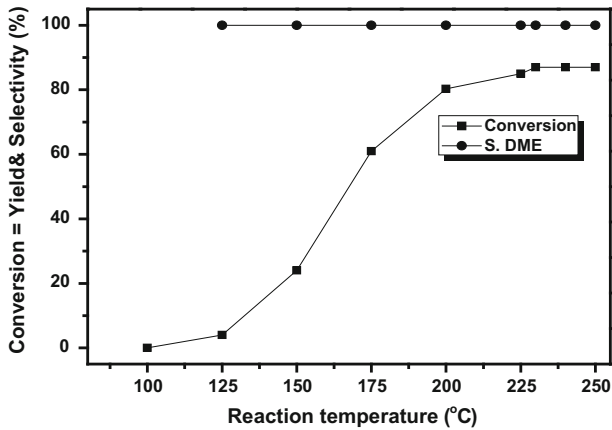


**Fig. 11** Variation of methanol conversion and DME yield with the reaction temperature over 1 % ZA catalyst calcined at 450 °C using air or nitrogen as a carrier gas

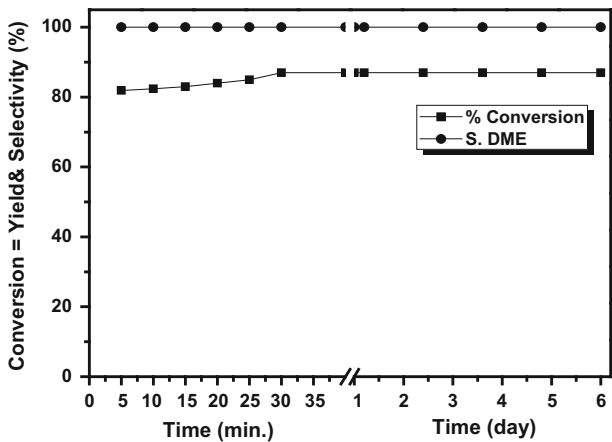


**Fig. 12** Variation of methanol conversion and DME yield with the reaction time over 1 % ZA catalyst calcined at 450 °C (at 230 °C reaction temperature)

and the methanol conversion and the yield of DME increase monotonically with increasing the reaction temperature up to 230 °C. With increasing the reaction temperature up to 250 °C, constant values of methanol conversion and yield of DME were obtained. Unfortunately, when the reaction temperature increased up to 275 °C in the presence of air as a carrier gas, the yield of DME drastically decreased due to oxidation of methanol to CO and CO<sub>2</sub> products. No oxidation of methanol was observed at 275 °C with a constant value of conversion and yield of DME in the presence of N<sub>2</sub> as a carrier gas. The above results indicate that the optimum reaction temperature for conversion of methanol to DME with 87 % yield and 100 % selectivity is at 230 °C under air or nitrogen as a carrier gas. Said et al. [16] studied

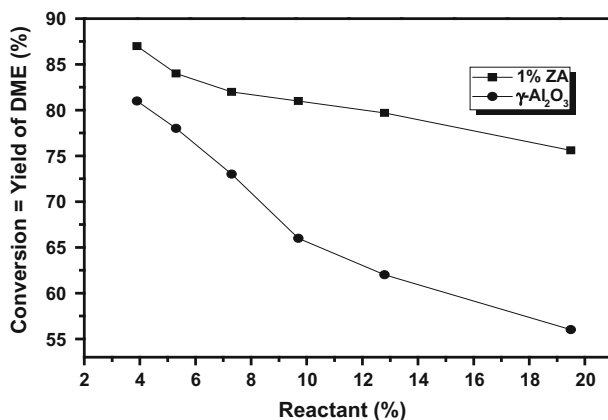


**Fig. 13** Variation of methanol conversion and DME yield with % reactant of methanol over  $\gamma$ -Al<sub>2</sub>O<sub>3</sub> calcined at 500 °C and 1 % ZA catalyst calcined at 450 °C (at 230 °C reaction temperature)

the catalytic performance of sulfated zirconia in dehydration of methanol to DME using air as a carrier gas. They stated that using air as a carrier gas prevented the deactivation of the sulfated zirconia catalyst.

#### *Catalyst stability test*

Because dehydration catalysts cannot be regenerated in situ, keeping high stability during a long-term reaction is very important [43]. The stability of 1 % ZA catalyst calcined at 450 °C was evaluated under the operating conditions of 230 °C, 1 atm, 500 mg catalyst and 50 ml flow rate for 6 days of time-on-stream using air or nitrogen as a carrier gas. Figure 12 shows that the dehydration reaction of methanol is very fast and the conversion of methanol reaches  $\approx 82$  % after 5 min. The reaction reaches a steady state of conversion after 30 min. Figure 12 also shows that the methanol conversion and selectivity to DME remained constant for 6 days, which indicates that no deactivation of the catalyst was occurring. This result reflects that the ZrO<sub>2</sub>-modified  $\gamma$ -Al<sub>2</sub>O<sub>3</sub> has good stability for the synthesis of DME from methanol under inert and oxidative atmospheres.

#### *Effect of % reactant*

The effect of % methanol reactant on the activity variation of  $\gamma$ -Al<sub>2</sub>O<sub>3</sub> calcined at 500 °C and 1 % ZA catalysts calcined at 450 °C were studied and the results are represented in Fig. 13, which shows that the higher activity towards DME formation is achieved at 4 % methanol over  $\gamma$ -Al<sub>2</sub>O<sub>3</sub> and 1 % ZA catalysts. The increase in value of % reactant led to an observable decrease in % conversion of methanol and consequently in the yield of DME. The figure also shows that, at a relatively high value of % reactant, the  $\gamma$ -Al<sub>2</sub>O<sub>3</sub> and 1 % ZA catalysts lost 26 and 11 % of their conversion of methanol, respectively. This means that the decrease in the

conversion of methanol over  $\gamma$ -Al<sub>2</sub>O<sub>3</sub> is more than that of 1 % ZA catalyst. These results again demonstrate that the 1 % ZA catalyst has excellent strength and stability of the active sites compared with that of pure nano- $\gamma$ -Al<sub>2</sub>O<sub>3</sub> catalyst.

## Conclusions

Structural data and catalytic activity measurements of ZrO<sub>2</sub>- $\gamma$ -Al<sub>2</sub>O<sub>3</sub> systems provide consistent information about important changes taking place in  $\gamma$ -Al<sub>2</sub>O<sub>3</sub> surface properties after the incorporation of ZrO<sub>2</sub>. Thus, from the results described above, it can be concluded that:

1. ZrO<sub>2</sub>- $\gamma$ -Al<sub>2</sub>O<sub>3</sub> systems are active and selective catalysts for the dehydration of methanol to DME at relatively low temperature (230 °C).
2. The maximum yield of DME ( $\approx$ 87 %) was obtained over 1 % ZA catalyst. This catalyst possessed a greater number of (L) acid sites, which are responsible for DME formation.
3. The ZrO<sub>2</sub>-modified  $\gamma$ -Al<sub>2</sub>O<sub>3</sub> has good stability for the synthesis of DME from methanol under inert and oxidative atmospheres.

## References

1. S.A. Hassanzadeh-Tabrizi, E. Taheri-Nassaj, J. Am. Ceram. Soc. **91**, 3546 (2008)
2. A. Krell, H. Ma, J. Am. Ceram. Soc. **86**, 241 (2003)
3. K. Tanabe, Mater. Chem. Phys. **13**, 347 (1985)
4. K. Tanabe, T. Yamaguchi, Catal. Today **20**, 185 (1994)
5. J. Ortiz-Landeros, M.E. Contreras-García, H. Pfeiffer, J. Porous Mater. **16**, 473 (2009)
6. R.H. Williams, E.D. Larson, Energy. Sustain. Dev. **7**, 103 (2003)
7. T.A. Semelsberger, R.L. Borup, H.L. Greene, J. Power Sources **156**, 497 (2006)
8. G.R. Moradi, F. Yaripour, P. Vale-Sheyda, Fuel Process. Technol. **91**, 461 (2010)
9. D. Varisli, K.C. Tokay, A. Ciftci, T. Dogu, G. Dogu, Turk. J. Chem. **33**, 355 (2009)
10. J.H. Kim, M.J. Park, S.J. Kim, Appl. Catal. A Gen. **264**, 37 (2004)
11. A. García-Trenco, A. Martínez, Appl. Catal. A: Gen. **411–412**, 170 (2012)
12. K.-W. Jun, H.S. Lee, H.-S. Roh, S.-E. Park, Bull. Korean Chem. Soc. **24**, 106 (2003)
13. J. Sun, G. Yang, Y. Yoneyama, N. Tsubaki, ACS Catal. **4**, 3346 (2014)
14. B.D. Cullity, *Elements of X-ray Diffraction*, 3rd edn. (Addison-Wesley, Reading, 1967)
15. A.I. Osman, J.K. Abu-Dahrieh, D.W. Rooney, S.A. Halawy, M.A. Mohamed, A. Abdelkader, Appl. Catal. B Environ. **127**, 307 (2012)
16. A.A. Said, M.M. Abd El-Wahab, M. Abd El-Aal, J. Mol. Catal. A: Chem. **394**, 40 (2014)
17. G. Li, W. Li, M. Zhang, K. Tao, Catal. Today **93–95**, 595 (2004)
18. E.A. García, E.H. Rueda, A.J. Rouco, Appl. Catal. A: Gen. **210**, 363 (2001)
19. T. Yamamoto, T. Tanaka, S. Takenaka, S. Yoshida, T. Onari, Y. Takahashi, T. Kosaka, S. Hasegawa, M. Kudo, J. Phys. Chem. B **103**(13), 2385 (1999)
20. T. Klimova, M.L. Rojas, P. Castillo, R. Contreras, J. Ramírez, Microporous Mesoporous Mater. **20**, 293 (1998)
21. S. Damyanova, P. Grange, B. Delmon, J. Catal. **168**, 421 (1997)
22. L. Zhang, N. Li, P. Fan, X. Chu, S. An, J. Zhang, X. Wang, Hydrometallurgy **127–128**, 8 (2012)
23. F. Heshmatpour, R.B. Aghakhanpour, Adv. Powder Technol. **23**, 80 (2012)
24. A. Sinhamahapatra, N. Sutradhar, M. Ghosh, H.C. Bajaj, A.B. Panda, Appl. Catal. A Gen. **402**, 87 (2011)
25. X. Dou, D. Mohan, U. Charles, J. Pittman, S. Yang, Chem. Eng. J. **198–199**, 236 (2012)

26. C. Li, Y.-W. Chen, T.-M. Yen, J. Sol-Gel. Sci. Technol. **4**, 205 (1995)
27. M. Moràn-Pineda, S. Castillo, T. López, R. Gómez, Cordero-Borboa, O. Navaro, Appl. Catal. B Environ. **21**, 79 (1999)
28. S.S. Chan, I.E. Wachs, L.L. Murrell, N.C. Dispenziere, JR. J. Catal. **92**, 1 (1985)
29. X. Gao, J.L. Fierro, I.E. Wachs, Langmuir **15**, 3169 (1999)
30. S. Brunauer, L.S. Deming, W.E. Deming, E. Teller, J. Am. Chem. Soc. **62**, 1723 (1940)
31. J.H. de Boer, E.P. Everette, F.S. Stone (eds.), *The Structure and Properties of Porous Materials* (Butterworths, London, 1958)
32. J.M. Dominguez, J.L. Hernandez, G. Sandoval, Appl. Catal. A Gen. **197**, 119 (2000)
33. S. Da Ros, E. Barbosa-Coutinho, M. Schwaab, V. Calsavara, N.R.C. Fernandes-Machado, Mater. Charact. **80**, 50 (2013)
34. J.R. Sohn, H.J. Jang, J. Mol. Catal. **64**, 349 (1991)
35. A.A. Said, J. Chem. Technol. Biotechnol. **78**, 733 (2003)
36. A.A. Said, M.M.M. Abd El-Wahab, A.M. Alian, J. Chem. Technol. Biotechnol. **82**, 513 (2007)
37. M. Ziolk, J. Kujawa, O. Saur, A. Aboulayt, J.C. Lavalley, J. Mol. Catal. A: Chem. **112**, 125 (1996)
38. F.M. Bautista, J.M. Campelo, A. Garcia, D. Luna, J.M. Marinas, M.C. Moreno, A.A. Romero, Appl. Catal. A: Gen. **170**, 159 (1998)
39. F.S. Ramos, A.M. Duarte de Farias, L.E.P. Borges, J.L. Monteiro, M.A. Fraga, E.F. Sousa-Aguiar, L.G. Appel, Catal. Today **101**, 39 (2005)
40. A. Khaleel, Fuel **90**, 2422 (2011)
41. J. Khom-in, P. Prasertdam, J. Panpranot, O. Mekasuwandumrong, Catal. Commun. **9**, 1955 (2008)
42. J.B. Miller, E.I. Ko, Catal. Today **35**, 269 (1997)
43. B. Sabour, M.H. Peyrovi, T. Hamoule, M. Rashidzadeh, J. Ind. Eng. Chem. **20**, 222 (2014)